Science of the Total Environment 831 (2022) 154921

Contents lists available at ScienceDirect

Science of the Total Environment

journal homepage: www.elsevier.com/locate/scitotenv

Role of subterranean microbiota in the carbon cycle and greenhouse gas dynamics

Tamara Martin-Pozas [a], Soledad Cuezva [b,c,*], Angel Fernandez-Cortes [d], Juan Carlos Cañaveras [e], David Benavente [e], Valme Jurado [f], Cesareo Saiz-Jimenez [f], Ivan Janssens [c], Naomi Seijas [a], Sergio Sanchez-Moral [a]

[a] Department of Geology, National Museum of Natural Sciences (MNCN-CSIC), 28006 Madrid, Spain
[b] Department of Geology, Geography and Environment, University of Alcalá, Scientific Technological Campus, 28802 Alcalá de Henares, Spain
[c] Plants and Ecosystems, Department of Biology, University of Antwerp, 2610 Wilrijk, Belgium
[d] Department of Biology and Geology, University of Almeria, 04120 Almeria, Spain
[e] Department of Environmental and Earth Sciences, University of Alicante, San Vicente del Raspeig Campus, 03690 Alicante, Spain
[f] Department of Agrochemistry, Environmental Microbiology and Soil Conservation, Institute of Natural Resources and Agricultural Biology (IRNAS-CSIC), 41012 Seville, Spain

HIGHLIGHTS

- Cave sediments provide ecosystem services related to carbon and nitrogen cycling.
- Cave sediments promote a continuous CH_4 consumption from subsurface atmosphere.
- Moonmilk is a cave deposit that captures and mineralizes atmospheric CO_2.
- Cave sediments promote continuous CO_2 emission, but during the stagnation stage, uptake-fixation processes are also detected.
- Moonmilk formation is related to syntrophic relationships between *Crossiella* and nitrifying bacteria.

GRAPHICAL ABSTRACT

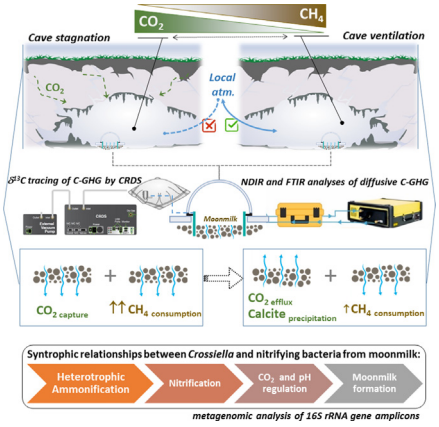

ARTICLE INFO

Editor: Fang Wang

Keywords:
Microbial activity
Subterranean ecosystems
Greenhouse gas fluxes
Moonmilk
Biomineralization

ABSTRACT

Subterranean ecosystems play an active role in the global carbon cycle, yet only a few studies using indirect methods have focused on the role of the cave microbiota in this critical cycle. Here we present pioneering research based on in situ real-time monitoring of CO_2 and CH_4 diffusive fluxes and concurrent $\delta^{13}C$ geochemical tracing in caves, combined with 16S microbiome analysis. Our findings show that cave sediments are promoting continuous CH_4 consumption from cave atmosphere, resulting in a significant removal of 65% to 90%. This research reveals the most effective taxa and metabolic pathways in consumption and uptake of greenhouse gases. Methanotrophic bacteria were the most effective group involved in CH_4 consumption, namely within the families *Methylomonaceae*, *Methylomirabilaceae* and *Methylacidiphilaceae*. In addition, *Crossiella* and *Nitrososoccaceae* wb1-P19 could be one of the main responsible of CO_2 uptake, which occurs via the Calvin-Benson-Bassham cycle and reversible hydration of CO_2. Thus, syntrophic relationships exist between *Crossiella* and nitrifying bacteria that capture CO_2, consume inorganic N produced by heterotrophic ammonification in the surface of sediments, and induce moonmilk formation. Moonmilk is found as the most

* Corresponding author at: Department of Geology, Geography and Environment, University of Alcalá, Scientific Technological Campus, 28802 Alcalá de Henares, Spain.
E-mail addresses: tmpozas@mncn.csic.es (T. Martin-Pozas), soledad.cuezva@uah.es (S. Cuezva), acortes@ual.es (A. Fernandez-Cortes), jc.canaveras@ua.es (J.C. Cañaveras), david.benavente@ua.es (D. Benavente), vjurado@irnase.csic.es (V. Jurado), saiz@irnase.csic.es (C. Saiz-Jimenez), ivan.janssens@uantwerpen.be (I. Janssens), nseijasmorales@mncn.csic.es (N. Seijas), ssmilk@mncn.csic.es (S. Sanchez-Moral).

http://dx.doi.org/10.1016/j.scitotenv.2022.154921
Received 13 January 2022; Received in revised form 15 March 2022; Accepted 26 March 2022
Available online 29 March 2022

evolved phase of the microbial processes in cave sediments that fixes CO_2 as calcite and intensifies CH_4 oxidation. From an ecological perspective, cave sediments act qualitatively as soils, providing fundamental ecosystem services (e.g. nutrient cycling and carbon sequestration) with direct influence on greenhouse gas emissions.

1. Introduction

While the role of marine and land-surface ecosystems as carbon sinks is unequivocal (Le Quéré et al., 2018), the contribution of subterranean ecosystems to the carbon greenhouse gas (C-GHG) budget is comparatively less studied. Subterranean ecosystems, including karst and lava tubes, are a significant part of the Earth's Critical Zone (Brantley et al., 2007), covering approximately 20% of the terrestrial surface (Ford and Williams, 2007; Chen et al., 2017) and acting as rapid CH_4 sink and as alternately CO_2 source or sink (Fernandez-Cortes et al., 2015a, 2015b; Waring et al., 2017). These systems host a great diversity of specialized organisms (Sánchez-Fernández et al., 2021) and contain abundant sedimentary deposits that host a significant fraction of the Earth's prokaryotic biomass, even at great depths (Magnabosco et al., 2018). The research background on the active role of microbial species in the exchange processes of C-GHG in subterranean environments is specifically related to: (i) removal of CH_4 from cave air by microbial methanotrophy, inferred mainly by indirect methods, as incubation of soil samples (Waring et al., 2017) and mesocosmos experiments (Lennon et al., 2017; Nguyễn-Thuỳ et al., 2017); and (ii) bioprecipitation of calcium carbonate deposits based on measurements of CO_2 sequestration or release from cave bacteria isolates in the laboratory (Okyay and Rodrigues, 2015). However, to our knowledge, there are no studies in the literature that address the direct in-situ measurement and monitoring of CO_2 and CH_4 fluxes from bacterial communities in caves. Field research based on in-situ CO_2 efflux measurements over *Actinobacteria* biofilms on cave rock surfaces was reported only by Cuezva et al. (2012), confirming that these bacteria promoted the uptake of CO_2 and later favored the precipitation of calcite crystals in periods of lower humidity.

Moonmilk deposits are the best known and widespread example of microbially-induced calcium carbonate precipitation (MICP) in different subterranean environments, from karstic (Cañaveras et al., 2006) and volcanic caves (Gonzalez-Pimentel et al., 2021) to granite tunnels (Miller et al., 2018). In fact, a growing research interest has recently been raised in the scientific community on understanding microbial communities and mechanisms involved in mineral precipitation processes (Maciejewska et al., 2017). The temporal and spatial ubiquity of moonmilk deposits in subsurface environments makes them excellent natural laboratories to study the role of microbial communities in gas exchange phenomena.

Here, we present a pioneering multidisciplinary study in Pindal Cave, Asturias, northern Spain (data in Fig. A1, Appendix A - Supplementary data) to determine: (i) the main active prokaryotic groups present in cave sediments and bio-induced deposits involved in mobilization, transformation, and storage of carbon (and nitrogen) in the subterranean environment; (ii) the most effective taxa and metabolic pathways involved in the uptake-fixation-production of CO_2 and CH_4; and (iii) the flux rates of these gases between sediments and the cave atmosphere under different bioclimatic conditions.

For this purpose, this research is based on the in-situ and real-time monitoring of diffusive fluxes using a closed chamber-based gas exchange system coupled with non-dispersive infrared and Fourier Transform Infrared gas analyzers, and concurrent $\delta^{13}C$ geochemical tracing by cavity ring-down spectroscopy. We evaluated and quantified CO_2 and CH_4 fluxes from cave sediments and moonmilk deposits directly exchanged with the cave atmosphere. Moonmilk and sediments are characterized by means of textural, mineralogical, geochemical and isotopic analyses ($\delta^{13}C_{bulk}$). Microbial communities present in cave sediments and moonmilk deposits were also characterized by metagenomic analysis of 16S rRNA gene amplicons in terms of composition and ecological functionality, particularly those related with the cycle of C-GHG (Fig. 5 and Appendix A – Supplementary data).

2. Methods

2.1. Site description and sampling

This study was conducted in Pindal Cave, which is located in Asturias (NW Spain), 4°30′ W, 43°23′ N (Fig. A1, Appendix A - Supplementary data). The geomorphology of this cave has been previously described by Jiménez-Sánchez et al. (2006). The cave has a single wide entrance near the coastline and is horizontally developed in the vadose zone of a karst massive modelled Carboniferous limestone located in a marine terrace (rasa) at 50–64 m above sea level. The total length of the cave is 590 m, but the tourist sector where this study has been performed is 341 m long, with an E-W orientation and an average width of 25 m.

We sampled three areas with a decreasing moonmilk development from A to C. Within these areas, we separated two types of samples by depth: 1) the most superficial (0–1 cm depth) layer where the main differences occurred; and 2) a deeper layer (1–3 cm depth) more homogeneous and without visible moonmilk development (Fig. 3). All samples were collected aseptically and stored at 4 °C until further analyses. The samples used for metagenomics were directly suspended in DNA/RNA Shield™ and stored at −80 °C until DNA extractions were performed.

2.2. Textural, mineralogical, geochemical and isotopic analyses

All sediment samples were crushed and sieved through a 2 mm sieve, and then ground to <60 mm for determination of sulfur (S) and trace elements. The pH of the sediments was measured in a 1:2.5 sample/H_2O extract, after shaking for 1 h, with a glass electrode. Total organic carbon (TOC) was analyzed by dichromate oxidation and titration with ferrous ammonium sulfate by the Walkley and Black method (Walkley and Black, 1934). Nitrogen (N) was determined by the Kjeldahl digestion method to convert organic nitrogen to ammonia. The digestate was alkalized, the ammonia distilled into boric acid and titrated with an acid of known concentration. For analysis of metal and trace element concentrations in sediment, samples were digested with aqua regia (1:3 conc HNO_3: HCl) in a microwave digester. Quantification of elements in the extracts was achieved using a VARIAN ICP 720-ES (simultaneous ICP-OES with axially viewed plasma). The accuracy of the analytical methods was assessed through BCR analysis (Community Bureau of Reference) and reference soil samples from the Wageningen Evaluating Programs for Analytical Laboratories for soils, International Soil-analytical Exchange (WEPAL, ISE).

$\delta^{13}C_{bulk}$ was analyzed by a combustion module (CM) coupled to a Cavity Ring-Down Spectroscopy (CRDS) System (G2201-i Analyzer, Picarro Inc., USA) at the University of Almeria (Spain). Samples of moonmilk and powdered sediment in tin capsules (~1.25 mg) were loaded into the CM by an autosampler (Costech, USA), achieving a complete combustion at 1200 °C. The CO_2 released passed through a water filter and a GC-column and was transferred to a Picarro Liaison™ A0301 interface and finally inputted into CRDS for analysis. The system assembly uses ultra-high purity (UHP) N_2 as the carrier gas and pure O_2 for combustion. Two L-glutamic acid standards: USGS40 ($\delta^{13}C$ VPDB = −26.4‰) and USGS41a ($\delta^{13}C$ VPDB = +37.6‰), supplied by USGS/Reston Stable Isotope Laboratory, were used to calibrate the CM-CRDS system. $NaHCO_3$ ($\delta^{13}C$ VPDB = −10.9‰), sugarcane ($\delta^{13}C$ VPDB = −11.7‰), acetanilide ($\delta^{13}C$ VPDB = −26.3‰) urea ($\delta^{13}C$ VPDB = −49.2‰) were used as working reference standards for consecutive rounds of $\delta^{13}C$ analyses. Four replicates per sample and per each standard were analyzed. Memory effects from previous samples were avoided by discarding the first analysis. $\delta^{13}C$-isotope values were normalized against the Vienna Pee Dee Belemnite (V-PDB, as ‰) scale by analyzing the working reference standards before and after

each batch of samples. Based on the reference standards analyses, the obtained repeatability was <0.22‰ (±1 SD, $n = 22$) with an accuracy of 0.11% (expressed as mean relative error).

2.3. Environmental monitoring and isotopic tracking of CO_2 and CH_4

Convective cave ventilation driven by temperature difference between the cave and the external environment was recorded over two annual cycles (from September 2017 to August 2019). Data were collected by a meteorological station outside and in-cave sensors, including the continuous monitoring of an inert trace gas as radon (^{222}Rn) and spatially-resolved measurements of the main C-GHG (CO_2 and CH_4). This continuous monitoring period comprised the seasonal field campaigns targeted for in-situ measurements of microbial fluxes rates of CO_2 and CH_4 and the coeval isotopic tracking of both gases, which technical procedure is addressed below.

In-cave sensors were placed at a height of 1 m at the end of the touristic gallery, 120 m far from the cave entrance and adjacent to the sampling locations of moonmilk and sediments. Air temperature was measured using a high-accuracy temperature logger with an external thermistor (SBE 56, Sea-Bird Electronics, USA). Radon concentration was recorded to characterize the cave ventilation dynamics using an AlphaE radon monitor (Bertin Tech., France) equipped with a diffusion chamber with silicon diode. Data were recorded at 5 min and 1 h intervals for cave air temperature and radon concentration, respectively, but with some gaps in the case of radon records due to electronic failures.

The weather conditions outside the cave were analyzed by using the hourly temperature data series from a meteorological station at San Vicente de la Barquera, belonging to the Spanish Meteorological Agency (Cantabria, Spain). This station is located near the coast line at 12 km far from Pindal Cave (35 m.a.s.l, 4°24′ W, 43°23′ N).

2.4. Real-time monitoring of CO_2 and CH_4 diffusive fluxes from cave sediments and moonmilk deposits

An in-situ real-time monitoring on top of moonmilk deposits was developed with a closed chamber-based gas exchange system, aimed to characterize CO_2 and CH_4 fluxes from moonmilk directly exchanged with the cave atmosphere. To this end, two fixed PVC collars (diameter 20 cm) were installed beforehand in the place fixed inside the cave (Fig. 3), one directly installed on top of the zone completely covered by moonmilk deposits (zone A) and the other one on the zone with no visible moonmilk deposits (zone C). In-situ measurement of CO_2 fluxes was conducted by using an Automated Soil Gas Flux System LI-8100A (LI-COR Biosciences, USA), equipped with a Long-Term Chamber 8100–104 (Fig. A4, Appendix A - Supplementary data). We performed flux measurements of 10 min every 15 min with 5-min intervals, measuring CO_2 (μmol per mol dry air) every second. In addition, the system allows air samples to be taken for analyzing the CO_2 and CH_4 molar fractions and $\delta^{13}C$ in both gases, using CRDS spectrometers.

From June 2018, in-situ measurements of C-GHG fluxes were performed by coupling Automated Soil Gas Flux System with a portable Fourier Transform Infrared (FTIR) spectrometer (DX4015, Gasmet Technologies, Finland) (Fig. A4, Appendix A - Supplementary data). The FTIR performs a multi-species analysis of gas mixture accumulated into the closed chambers and it is specifically factory-calibrated for the C-GHG concentrations and vapor contents usually found in cave atmospheres, achieving detection limits better than 1 ppm. To compute CO_2 and CH_4 flux measurements and analyze data results we used SoilFluxPRO™ Software.

In order to evaluate the effect of the states of ventilation inside the cavity, the monitoring campaigns were developed in the different seasonal patterns; cave ventilation stage and cave stagnation stage.

An isotopic tracking of CO_2 and CH_4 becomes crucial for a genetic diagnosis and for assessing the dynamic and lifetime of both gases in the cave environment and, particularly, in relation with bio-induced moonmilk deposits and the underlying cave sediments. For this purpose, grab samples were collected, on a quarterly basis, from cave air and gas mixture accumulated into the closed chambers used for measuring microbial fluxes, as well as from the background atmosphere and soil at exterior overlying soil. Air samples were collected and immediately stored in 1-L RITTER gas sampling bags. These air samples were analyzed within 48 h for CO_2 and CH_4 molar fractions and $\delta^{13}C$ in both gases, using CRDS spectrometers (G2201-i analyzer, Picarro Inc., USA) at the laboratories of stable isotopes of National Museum of Natural Sciences and University of Almeria. Three in-house standards with certified CO_2 and CH_4 concentrations and known $\delta^{13}C$ values for each gas were processed to verify the proper functioning of the CRDS analyzer. Fernandez-Cortes et al. (2015a, 2018) reported further details on the methodological procedures for air sampling and CRDS analyses, including data concerning the quality of the results in terms of precision and accuracy.

2.5. DNA extraction, bacterial 16S rRNA amplicon sequence libraries and bioinformatics pipeline

DNA was extracted from 300 to 500 mg of samples using the FastDNA SPIN Kit for soil (MP Biomedicals, France) according to manufacturer instructions. The DNA concentrations were quantified by using a Qubit 2.0 fluorometer (Invitrogen, USA). We amplified the V3 and V4 regions of the 16S ribosomal RNA to characterize prokaryota communities for all samples using Illumina MiSeq and 2 × 250 paired end sequencing. The primer sequences used in this study were 341F and 805R (Herlemann et al., 2011).

Raw data were processed with QIIME2 version 2019.10 (Bolyen et al., 2019). Quality control and trimming were performed using FASTQC. The Cutadapt package was used to remove PCR primers and the Deblur package was used to truncate the low-quality readings, with a PHRED score below 20 (Amir et al., 2017). Taxonomic assignment has been performed by querying the sequence reads against the SILVA SSU 132 reference database (Quast et al., 2013), using the feature-classifier classify-sklearn method implemented in QIIME2 (Bokulich et al., 2018). The sequencing data was processed using the phyloseq R package (McMurdie and Holmes, 2013). All analyses were performed using R v3.6.0. Ecological alpha diversity was calculated using Shannon and Simpson diversity indices. Exclusive and shared ASVs between samples were detected using the Upset tool in R (Lex et al., 2014). Spearman's correlation among the most abundant bacterial taxa (with ≥ 0.5% read in at least one samples) was performed using rcorr function of Hmisc and corrplot function in R package (Fig. A5, Appendix A - Supplementary data). Correlation coefficients >0.6 and P-value <0.05 were imported in Cytoscape software. The open source software Cytoscape 3.9.1 was employed to visualize the most abundant genera based on their relative abundances.

The PICRUSt2 software was used to generate predictions of gene function based on the 16S rRNA gene data for Enzyme Classification numbers (EC numbers), and infer MetaCyc pathway abundances using the PICRUSt2 full pipeline (Douglas et al., 2019). Sequences with Nearest Sequenced Taxon Index (NSTI) values above 0.3 were excluded from the analysis. The inferred pathway abundances were used to generate a heat-map using the "pheatmap" library in R package. Additionally, EC numbers abundances of genes related to bio-precipitation, carbon dioxide capture, aerobic respiration, nitrogen and CH_4 metabolism were extracted from EC number metagenome predictions and shown in Fig. 5 and Tables A5 and A6 (Appendix A - Supplementary data).

2.6. Data availability

The 16S rRNA gene sequences and accompanying metadata have been deposited in the Sequence Read Archive (SRA) of NCBI under the project number PRJNA780369.

3. Results and discussion

3.1. Climate-driven ventilation controlling the composition of cave gases

The geographical area of Pindal Cave is characterized by an oceanic climate, humid with a temperate summer, exhibiting diurnal and seasonal

temperature cycles that contrast with the relatively constant cave temperature over an annual cycle (11.62 °C ± 0.55 °C). The relative temperature variations between the cave and the external environment drive bi-directional convective airflow through the cave, primarily through the wide entrance near the coastline, which also plays a crucial role in determining the concentrations of cave gases.

The daily temperature of the local atmosphere compared to the temperature and ^{222}Rn content of cave air are shown in Fig. 1, highlighting the dates when in situ measurements of C-GHG fluxes and sampling were conducted. A stair-step pattern with sharp seasonal shifts of cave trace gas concentrations (^{222}Rn) is distinguishable. Firstly, a ventilation stage, with a remarkable pulses of cave air renewal that provokes a depletion of ^{222}Rn concentration up to reach minimum levels (usually below 1000 Bq m^{-3}) during the colder months (particularly, from December to March). Secondly, a stagnation stage of the cave atmosphere during the warmer and drier months (from May to October), characterized by a steady accumulation of ^{222}Rn in the cave atmosphere up to reach monthly-averaged values constantly higher than 3000 Bq m^{-3}. The ventilation stage begins and ends when the temperature gradient between the cave and the external environment is continuously reversing (usually during April and November). The transition between stages occurs when the temperature outside is distinctly above or below the annual mean of cave air temperature, triggering the prevailing recharge or dilution of gases from the cave atmosphere, respectively.

The CO_2 was also tracked through analyzing its molar fraction and $\delta^{13}C$ from air samples collected at a predefined network of points into the cave, from the entrance to the deepest zones, as well as from the porous system of soil and local background atmosphere at the exterior. The well-recognized model for CO_2 sourcing in cave atmospheres establishes the concentration and isotopic ratio of the CO_2 observed in each cave location results from the proportional mixing of the background atmosphere and a second source with an isotopically light CO_2-rich component, accordingly to a Keeling approach based on a simplified two-end member linear function (Pataki et al., 2003). This second CO_2 source to the cave atmosphere does not necessarily correspond to a single pure-CO_2 end-member, but instead gas would come from a combination or alternation of sources. CO_2 enters the cave by diffusion directly from the overlying soil or the surrounding vadose crevices, air-filled voids and other connected porosity of the bedrock (i.e., CO_2-enriched "ground-air" reported by Mattey et al. (2016), or CO_2-degassing from seepage water feeding the cave environment.

Keeling diagram ($1/CO_2$ versus $\delta^{13}C$-CO_2) for the external atmosphere–overlying soil–cave system (Fig. 2) enables us to distinguish the prevalence of potential sources of CO_2 into the cave environment through the intercept value of the lineal Keeling function in the $\delta^{13}C$-CO_2 axis (Garcia-Anton et al., 2017). The $\delta^{13}C$-CO_2 estimated for isotopically light CO_2-rich end-member was almost the same (roughly −25.50‰) for the two seasonal patterns distinguished in function of the trace gas concentrations, in function of the temperature difference between cave air and the outside and the seasonal variations of radon concentration, namely ventilation and stagnation stages (Fig. 1). The $\delta^{13}C$-CO_2 value for light CO_2-rich end-member during the ventilation stage ranged from −24.12 to −27.38‰ (intercept values by the dashed straight lines from Fig. 2), indicating that CO_2 primarily results from the root and microbial respiration in soils containing organic matter from C3 vegetation (with $\delta^{13}C$-CO_2 ranging −25.0 to −27.5‰) (Cerling et al., 1991; Davidson, 1995; Kuzyakov, 2006). This soil-derived CO_2 diffuses into the cave atmosphere, where it is diluted with the external ^{13}C-enriched atmospheric CO_2 entering by convective airflow. The estimated range for the light CO_2-rich end-member evinces that, on the one hand, there is not any significant contribution of ^{13}C-enriched CO_2 through both equilibrations with the Dissolved Inorganic Carbon (DIC) in the vadose water either the oxidation of organic material washed down into the vadose zone (Mattey et al., 2021), and on the other hand, nor a signal towards a light CO_2 evolved from degassing, i.e. due to drip water or prior calcite precipitation.

3.2. Bacterial communities on cave formations: From sediments to emerging and well-developed moonmilk deposits

Three types of surface were studied: sediments without moonmilk deposits and sediments with moonmilk deposits corresponding to the initial phase of moonmilk formation (Cañaveras et al., 2006) with two different degrees of development (Fig. 3). The locations (A,B,C) illustrates the different bacterial composition between surface sediments (A1, B1, C1) and deep sediments (A2, B2, C2). Under scanning electron microscopy, moonmilk

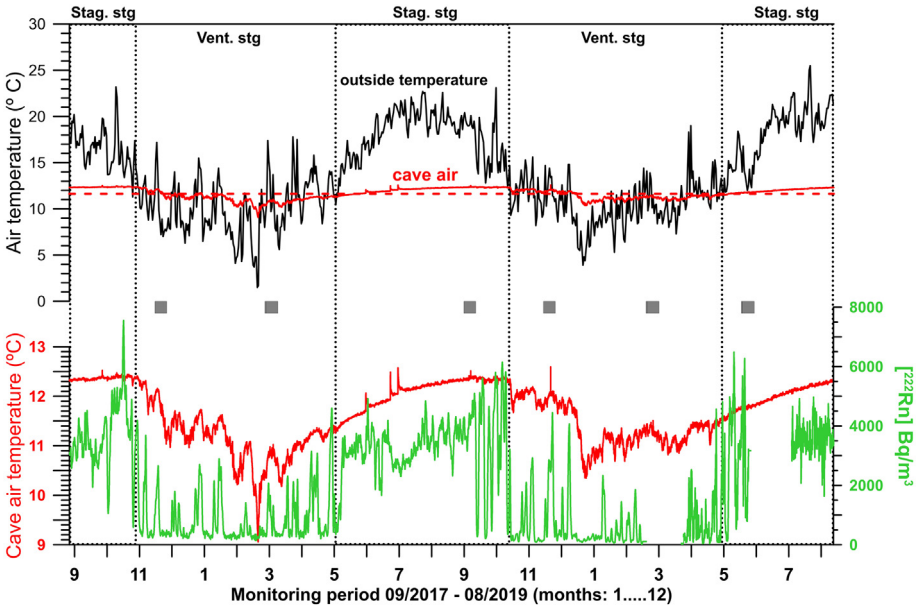

Fig. 1. Upper panel: time evolution of the air temperature difference between the cave air and the local atmosphere at Pindal Cave. The dashed red line represents the average cave temperature. Lower panel: seasonal and short-term variations of radon concentration (^{222}Rn) and temperature of cave air. Monitoring period: September 2017 – August 2019. The campaigns for gas-flux monitoring and grab sampling for isotopes analyses are marked as grey squares. The temperature gradient (cave-exterior) and concentration of the trace gas (^{222}Rn) allow for segmentation of the monitoring period on a seasonal sequence of ventilation and stagnation stages (Vent. stg and Stag. stg, respectively).

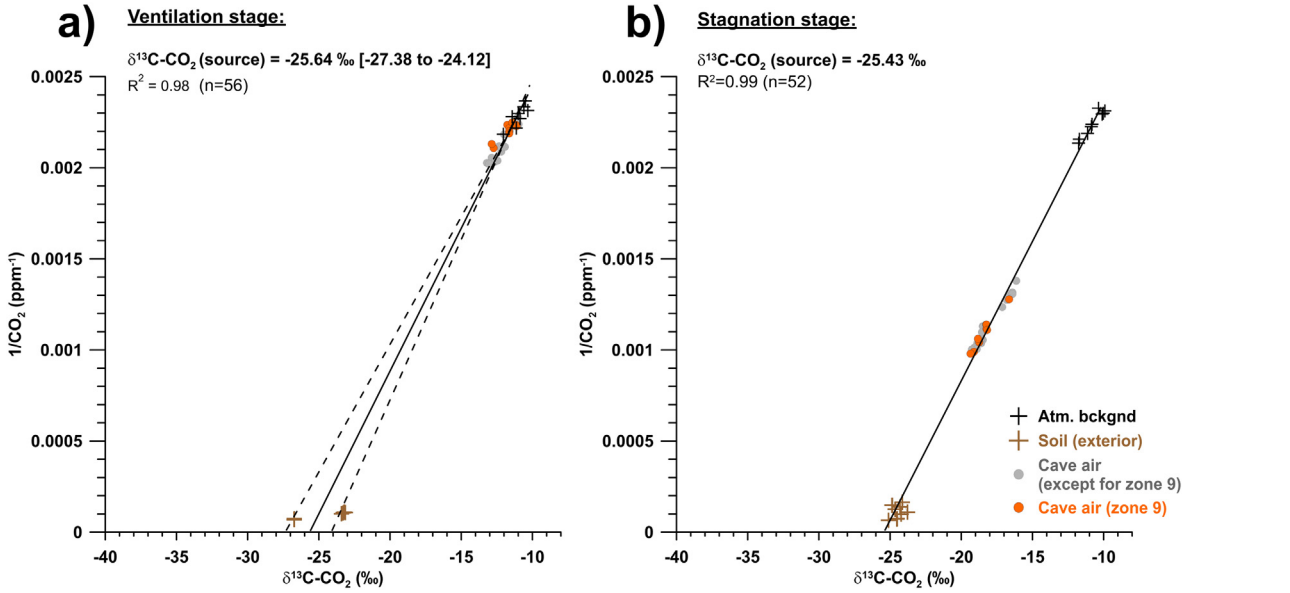

Fig. 2. Keeling diagrams, $\delta^{13}C\text{-}CO_2$ (‰) Vs $1/CO_2$ (ppm^{-1}), for the set of three environments, namely: local atmosphere – overlying soil outside the cave – cave system, and under two opposite gas-exchange settings with the exterior: (a) ventilation stage and (b) stagnation stage. Cave air samples labelled as zone 9 were collected in the moonmilk and sediment-sampling zone (see the study area marked in the Fig. A1, Appendix A – Supplementary data).

samples A1 and B1 presented monocrystalline needle-fiber calcite (NFC) networks and *Actinobacteria*-like filaments ranging 0.50–0.70 and 0.16–0.25 μm thick, respectively (Fig. 3 and Fig. A2, Appendix A - Supplementary data). The main difference between A1 and B1 originated in the development of calcite fibers: A1 presented a dense calcite fiber network, while B1 was an emerging moonmilk with a lower content of calcite fibers. Moreover, we found some overgrowths in calcite fibers of A1, the sample with moonmilk higher development. The calcite fibers overgrowth indicates that sample A1 corresponded to more ancient moonmilk stage than B1. The surface of sample C1, corresponding to the sediment without visible moonmilk deposits, showed only few *Actinobacteria*-like filaments and almost no calcite fibers.

The analyzed cave sediments were slightly alkaline, with pH ranging from 7.34–7.64 (Table A1, Appendix A - Supplementary data). X-ray diffraction analysis revealed a fine cohesive sediment deposit composed of quartz, calcite and phyllosilicates. The calcite content was higher in the sediment with higher moonmilk development, while calcite presence was lower in the layers below the moonmilk (Table A2, Appendix A - Supplementary data). All samples showed a high microbial diversity and shared the vast majority of amplicon sequence variants (ASVs) obtained by high-throughput 16S rRNA gene sequencing. We did not observe significant variations in the alpha diversity of the bacterial communities (Table A3 and Fig. A3, Appendix A - Supplementary data). Remarkably, the comparative study of the upper and lower layers of cave sediments showed a clear stratification of bacterial communities, which is related to the development of the moonmilk deposits (Fig. 3). *Actinobacteria* was one of the most abundant phyla in surface samples (16.5–36.4%), whereas their presence decreased drastically in the deepest sediment layers (5.6–10.4%) (Fig. 3 and Table A4, Appendix A - Supplementary data). The relative abundance of *Crossiella*, the most representative genus of *Actinobacteria*, was notably higher in sediments covered by moonmilk. Our results were consistent with previous moonmilk microbiome studies where *Actinobacteria* represented a high percentage of the moonmilk bacterial community (Maciejewska et al., 2018; Park et al., 2020). To the best of our knowledge, there is no study associating *Crossiella* relative abundance with moonmilk formation, except in the study on a volcanic cave where *Crossiella* relative abundance was 2.5% (Gonzalez-Pimentel et al., 2021). However, a few authors reported the finding of *Crossiella* not only in carbonate environments such as weathered rock caves (Ma et al., 2021), but also in deteriorated stone monuments (Li et al., 2018).

The lineage wb1-P19, within the order *Nitrosococcales,* (*Proteobacteria*) was predominant in surface layers (11.2–6.9%), especially in those with visible moonmilk colonization. However, its proportion decreased below 5% in the deepest sediment layer (Fig. 3 and Table A4, Appendix A - Supplementary data). The lineage wb1-P19 was phylogenetically clustered with autotrophic nitrite oxidizing bacteria and frequently found in caves associated to microbial mats, moonmilk and water (Holmes et al., 2001; Riquelme et al., 2015; Park et al., 2020). In addition, we observed an increase of the heterotrophic phyla *Acidobacteria* and *Planctomycetes* in samples without moonmilk development (Fig. 3 and Table A4, Appendix A - Supplementary data). Both phyla are cosmopolitan and appeared frequently in oligotrophic sediments, but there exists relatively little information about their ecological role (Eichorst et al., 2018; Ma et al., 2021). Collectively, our findings suggest that moonmilk deposit formation in Pindal Cave is closely related to *Crossiella* and wb1-P19. Additionally, the presence of *Crossiella* in cave sediments with no visible moonmilk colonization could indicate a potential zone of moonmilk development. Further, we also applied a profile clustering network analysis (Fig. 4) to obtain a deeper insight into syntrophic correlations between bacterial groups in moonmilk and sediments. Most abundant ASV were selected (with ≥ 0.5% read in at least one samples). The network analysis generated by a Cytoscape network showed the most abundant ASVs and highlighted the relative distribution and abundances. The network analysis and the Spearman rank correlation coefficient (Fig. A5, Appendix A - Supplementary data) confirmed previous observations, i.e.: strong positive correlations between *Crossiella* and wb1-P19, the most abundant sequences in moonmilk samples.

From these results, several important questions arise: Are the differences between sediment microbial communities with and without moonmilk deposits determining the rate of carbonate bioprecipitation? Do they influence gas exchange fluxes and ultimately the composition of the underground atmosphere? What are the taxa and metabolic pathways involved in consumption and uptake of C-GHG?

To solve these questions, we explored the sources and dynamics of C-GHG in two different microenvironments: cave sediments covered by moonmilk deposits (zone A in Fig. 3a) and bare cave sediments, not covered by moonmilk deposits (zone C in Fig. 3a). Likewise, we explored the variability of C-GHG fluxes during both the ventilation and stagnation cave stages.

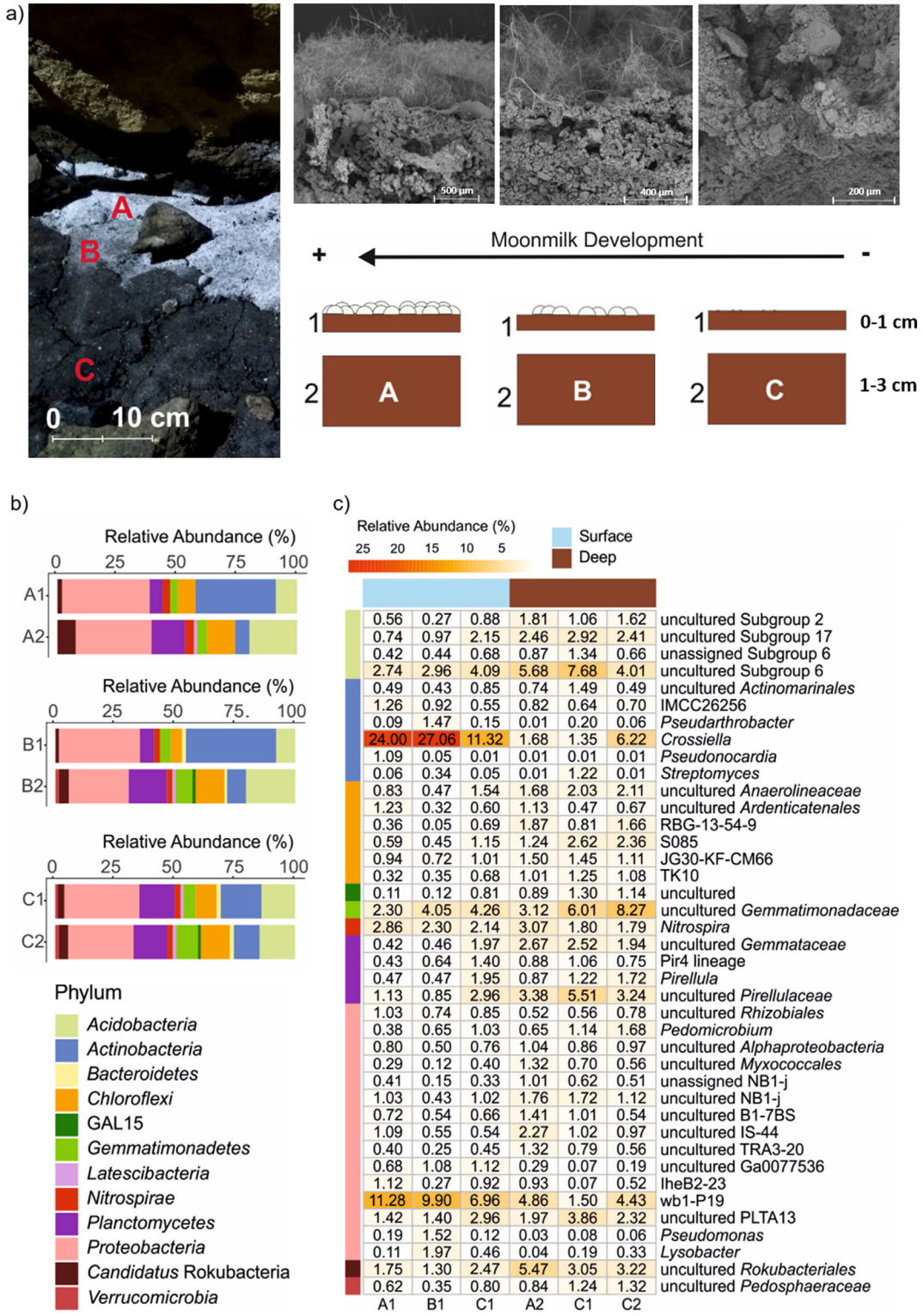

Fig. 3. (a) Examples of the different cave deposits that were analyzed in this study (A: well-developed moonmilk, B: emerging moonmilk and C: bare cave sediment). (b) Relative abundances of the most abundant bacterial phyla (with abundance >1%) from moonmilk deposits and sediments at different depths. (c) Heat map representing the relative abundances of *Bacteria* at the genus level. The genera with abundances below 1% were omitted. Genera are displayed on the Y axis, samples on the X axis. Colors from white to red indicate least to most abundant genera.

3.3. In situ exploration of sources and exchange rates of carbon-GHG fluxes between sediments and cave air

The in situ real time monitoring of carbon GHG fluxes by a closed chamber-based gas exchange system on top of moonmilk and cave sediments has provided remarkable data concerning CO_2 and CH_4 production and uptake inside the cave. The pattern of carbon gas exchange with the cave atmosphere recorded over the moonmilk was clearly different from that over bare cave sediment. Moreover, a variability in carbon fluxes was observed from successive survey

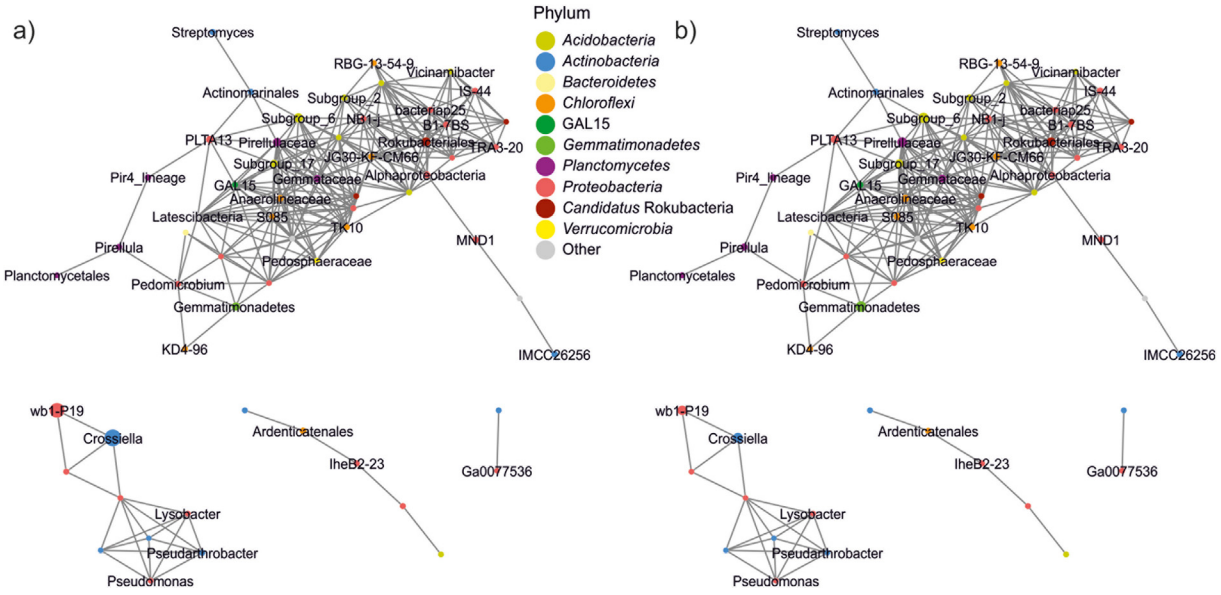

Fig. 4. Co-occurrence network deduced from most ASV relative abundance in moonmilk and sediment samples. Edges represent Spearman's rank correlation coefficient > 0.6, adjusted $P < 0.05$. Size of nodes represent the relative abundance in a) moonmilk and b) sediment samples.

campaigns corresponding to different ventilation conditions in Pindal Cave.

3.3.1. CO_2 fluxes from moonmilk deposits and bare cave sediments

During the cave ventilation stage, when CO_2 concentration in the cave atmosphere was similar to the free atmosphere, CO_2 emission fluxes (positive fluxes) were detected on top of the zone completely covered by moonmilk deposits (zone A) (Table 1). The daily-averaged CO_2 flux ranges from 0.06 to 0.08 $\mu mol \cdot m^{-2} \cdot s^{-1}$, with low daily variations in magnitude (average standard deviation 0.01 $\mu mol \cdot m^{-2} \cdot s^{-1}$, and 0.06 $\mu mol \cdot m^{-2} \cdot s^{-1}$ maximum daily range). By converting the value of the CO_2 flux emitted over 10 min (measured in moles), into values of total mass of gas emitted for each 10-min interval (in grams), we calculated the total net production (total mass emitted) of CO_2 on top moonmilk in 10–12 $mg \cdot m^{-2} \cdot h^{-1}$ and

Table 1
Statistics summary of the CO_2 and CH_4 fluxes measured on top of the moonmilk deposit and bare soil at the selected study area (Fig. A1) for a daily cycle. Sampling dates represent several different ventilation conditions, ventilation versus stagnation, over the annual cycle; N: number of measurements; Time interval: time of continuous measurement; [gas]: gas concentration in the cave atmosphere, ppm; F-gas: diffusive flux, $\mu mol \cdot m^{-2} \cdot s^{-1}$ for CO_2, and $nmol \cdot m^{-2} \cdot s^{-1}$, for CH_4; gas Net flux: estimated gas net production, $mg \cdot m^{-2} \cdot h^{-1}$ (avg/h), $mg \cdot m^{-2} \cdot day^{-1}$ gas total per day (Day); $\delta^{13}C$-gas: $\delta^{13}C$ of the gas on average, and standard deviation; avg.: average; max: maximum; min: minimum; sd: standard deviation.

CO_2 Flux

	Date	[CO_2]		Diffusive CO_2 flux				CO_2 Net flux		$\delta^{13}C$-CO_2	
	mm/yy	avg	sd	avg	avg sd	max	min	avg/h	Day	avg	sd
Ventilation	Moonmilk										
	03/18	443	14	0.06	0.01	0.09	0.03	10	244	−12.31	0.16
	11/17	423	3	0.08	0.01	0.09	0.07	12	292	−11.60	0.37
	Bare sediment										
	03/19	441	1	0.26	0.01	0.27	0.25	41	981	−11.66	–
	11/17	440	2	0.17	0.01	0.18	0.15	27	643	−12.82	–
Stagnation	Moonmilk										
	06/18	992	25	−0.01	0.03	0.04	−0.06	−0.9	−22	−19.04	0.11
	12/18	781	5	−0.04	0.02	−0.02	−0.06	−6.1	−147	−16.86	–
	Bare sediment										
	06/19	655	21	0.16	0.02	0.18	0.12	25	592	−14.54	0.45
	06/19	650	52	0.15	0.09	0.44	0.04	24	568	−14.00	0.26

CH_4 Flux

	Date	[CH_4]		F- CH_4				CH_4 Net flux		$\delta^{13}C$-CH_4	
	mm/yy	avg	sd	avg	avg sd	max	min	avg/h	Day	avg	sd
Ventilation	Moonmilk										
	03/19	1.85	0.18	−1.48	0.000	−1.48	−1.48	−0.09	−2.05	−44.48	–
	Bare sediment										
	03/19	1.71	0.12	−1.52	0.36	−1.26	−1.77	−0.09	−2.10	−45.69	–
Stagnation	Moonmilk										
	09/18	0.55	0.05	−1.90	1.07	1.58	−4.41	−0.11	−2.63	−23.44	2.62
	06/18	0.53	0.07	−1.26	0.30	−0.66	−2.38	−0.07	−1.75	−32.60	–
	Bare sediment										
	06/19	0.37	0.06	−0.82	1.63	2.22	−4.65	−0.05	−1.20	−23.64	2.88
	06/19	0.44	0.26	−0.63	1.16	1.87	−4.39	−0.04	−0.89	−30.73	1.03

from to 292 $mg{\cdot}m^{-2}{\cdot}day^{-1}$. On top of the bare cave sediment, with no visible moonmilk deposit (zone C), we detected CO_2 emission fluxes (positive fluxes). Comparing the same survey campaigns, the magnitudes are higher over the bare sediment than over the moonmilk: e.g. 0.17 vs 0.08 $\mu mol{\cdot}m^{-2}{\cdot}s^{-1}$, in November 2017. The 24-h net production estimated from the hour-averaged CO_2 net flux was higher directly above the bare cave sediment than on top of the moonmilk deposit: e.g. 643 $mg{\cdot}m^{-2}{\cdot}day^{-1}$ above the sediment versus 292 $mg{\cdot}m^{-2}{\cdot}day^{-1}$ above the moonmilk in 2017 November.

During the stagnation stage, in a CO_2-enriched cave atmosphere, CO_2 emission fluxes above the bare cave sediment have a daily-averaged of 0.15 $\mu mol{\cdot}m^{-2}{\cdot}s^{-1}$ with higher daily variations reaching a standard deviation of 0.09 $\mu mol{\cdot}m^{-2}{\cdot}s^{-1}$, on average, and up to 0.4 $\mu mol{\cdot}m^{-2}{\cdot}s^{-1}$ maximum diurnal amplitude. F_{CO2} have similar range values to those measured in the same zone under ventilation conditions. However, on top of the zone completely covered by moonmilk deposit, CO_2 fluxes are less than under ventilation, with predominance of CO_2 uptake (negative fluxes) (up to -0.04 $\mu mol{\cdot}m^{-2}{\cdot}s^{-1}$, on a daily average). Moreover, daily variations are higher in magnitude, with a mean standard deviation of 0.02–0.03 $\mu mol{\cdot}m^{-2}{\cdot}s^{-1}$ that reaches up to 0.10 $\mu mol{\cdot}m^{-2}{\cdot}s^{-1}$ maximum daily range. Most campaigns performed during stagnation stage showed significant temporal variability in flux intensity over the daily timescale above the moonmilk deposit, alternating emission or uptake, or fluctuating around zero throughout the day. The variation in the CO_2 concentration gradient between the cave sediment or moonmilk and the cave air regulates the diffusion intensity on a daily basis.

The 24-h net CO_2 balance, estimated from the hour-averaged CO_2 net flux, above the bare cave sediments was lower in the stagnation than in the ventilated stage (below 600 $mg{\cdot}m^{-2}{\cdot}day^{-1}$). Due to the stagnation of the subterranean atmosphere, the CO_2 concentration gradient between the cave sediment and the cave air was lower, and the diffusion intensity was slightly reduced. In any case, the data are also indicative of on-site active production of CO_2 in the bare cave sediment. The CO_2 daily net balance was significantly lesser on top of the moonmilk deposits. In fact, in several campaigns the daily balance was negative, representing a CO_2 capture/uptake of up to 147 $mg{\cdot}m^{-2}{\cdot}day^{-1}$.

3.3.2. CH_4 fluxes from moonmilk deposits and bare cave sediment

The CH_4 fluxes exchanged with the cave atmosphere from moonmilk deposits and bare cave sediments have provided negative values in all the surveys performed (Table 1). The results are clearly indicative of on-site active uptake of CH_4 from both cave substrata, extended in the annual term.

During the cave ventilation stage, CH_4 uptake fluxes of similar intensity on top of the moonmilk deposit (zone A) and on top of the zone with no visible colonization (zone C). The daily-averaged CH_4 flux was 1.5 $nmol{\cdot}m^{-2}{\cdot}s^{-1}$ in both cases, the CH_4 net uptake was around 0.09 $mg{\cdot}m^{-2}{\cdot}h^{-1}$ and the 24-h total CH_4 net uptake estimated was 2.1 $mg{\cdot}m^{-2}{\cdot}day^{-1}$.

During the cave stagnation stage, in a CH_4-depleted cave atmosphere, CH_4 uptake fluxes above the bare cave sediment are less intense compared to the ventilation stage: the value of the negative flux is halved to around -0.8 $nmol{\cdot}m^{-2}{\cdot}s^{-1}$ daily-averaged CH_4 flux. The 24-h total CH_4 net uptake was reduced by half -1.2 $mg{\cdot}m^{-2}{\cdot}day^{-1}$.

Above the moonmilk deposits, CH_4 uptake flux increased in the stagnation stage up to -1.9 $nmol{\cdot}m^{-2}{\cdot}s^{-1}$ daily-averaged CH_4 flux, with a mean standard deviation of 0.3–1.1 $nmol{\cdot}m^{-2}{\cdot}s^{-1}$ that reaches up to 2.8 $nmol{\cdot}m^{-2}{\cdot}s^{-1}$ maximum daily range. The CH_4 net uptake oscillated around 0.1 $mg{\cdot}m^{-2}{\cdot}h^{-1}$ and consequently the 24-h total estimated CH_4 net uptake 1.7–2.6 $mg{\cdot}m^{-2}{\cdot}day^{-1}$.

3.4. Role of the microbial community in greenhouse gases exchange fluxes between sediments and cave air

Regarding CO_2 fluxes, cave sediments do not exhibit any circadian rhythm, in contrast to surface soils or plant activity, likely because they do not experience noteworthy daily variations of temperature, moisture or irradiation. Conversely, at the seasonal scale, net CO_2 exchange between bare (without moonmilk) cave sediments and cave atmosphere is controlled by the seasonal variations in the gaseous composition of the subterranean atmosphere induced by the alternation of ventilation (cold seasons) and stagnation (warm seasons) stages that is typical for caves (James et al., 2015) (Figs. 1 and 2).

The long-term CO_2 flux measurements revealed a continuous one-way efflux from cave deposits into the open cave atmosphere. This CO_2 flux was clearly higher during the ventilation stage due to the greater concentration gradient between sediments and the cave's atmosphere (Table 1). Enzymes involved in the degradation of organic matter in cave sediments and cytochrome-c oxidase, involved in energy production, were predicted by PICRUSt2 for almost all dominant bacterial groups. It implies that the community from all samples was mainly composed of aerobic bacteria which produce CO_2 by the oxidative process that occurs during aerobic respiration (Fig. 5 and Table A5, Appendix A – Supplementary data). The respired CO_2 from these communities is then released to the cave sediments porous system and, ultimately, into the cave atmosphere mainly by diffusion.

However, CO_2 gas exchange with the cave atmosphere was clearly different between moonmilk deposits and bare cave sediments. In moonmilk deposits, very low CO_2 effluxes were registered during the ventilation stage, ranging from 0.06 to 0.08 $\mu mol{\cdot}m^{-2}{\cdot}s^{-1}$, while CO_2 fluxes during the stagnation stage were close to zero or slightly negative (Table 1). In contrast, in bare cave sediments, much larger positive CO_2 fluxes (emission fluxes) were constantly registered throughout the year, ranging from 0.15 to 0.26 $\mu mol{\cdot}m^{-2}{\cdot}s^{-1}$ (Table 1), i.e. more than twice the maximum flux rates registered on the moonmilk surfaces during the ventilation stage. CO_2 efflux from a moonmilk-producing surface is therefore much smaller than from a bare sediment. The lower fluxes in moonmilk imply either the CO_2 uptake process during carbonate precipitation or the lower production of CO_2 due to more anaerobic conditions under the moonmilk deposits.

During the stagnation stage the CO_2 efflux from cave sediments decreased. Under the stable environmental conditions prevailing in the stagnation stage, very low CO_2 uptake (negative flux) was typically observed in the moonmilk zone (-0.01 to -0.04 $\mu mol{\cdot}m^{-2}{\cdot}s^{-1}$; Table 1), in contrast to the sustained CO_2 emission (positive flux) recorded on bare sediments (averaging 0.15 $\mu mol{\cdot}m^{-2}{\cdot}s^{-1}$). These observations confirmed an effective CO_2 uptake by moonmilk bacterial communities consistent with predicted community functions, where phyla with CO_2 fixation capacity showed a relatively higher abundance in the sediment layers with moonmilk deposits (Fig. 5 and Table A5, Appendix A – Supplementary data). The functional predictions suggested a high abundance of carbonic anhydrase (CA) (Cuezva et al., 2012). The functional predictions suggested a high abundance of carbonic anhydrase (CA), which catalyze the reversible hydration of carbon dioxide ($CO_2 + H_2O \Leftrightarrow HCO_3^- + H^+$) in plants but also is found in autotrophic and heterotrophic microorganisms. Carbonic anhydrase enzymes (CAs) are involved in pH homeostasis, secretion of electrolytes, photosynthesis, carbon fixation, capturing atmospheric CO_2 and calcification process (Cuezva et al., 2012; Supuran and Capasso, 2017; De Goeyse et al., 2021; Yang et al., 2021; Steger et al., 2022). In Pindal Cave, PICRUSt2 predicted that CA was the most abundant enzyme involved in CO_2 uptake in almost all dominant bacterial groups but the higher abundances were associated to *Crossiella* and wb1-P19, the dominant genera in moonmilk (Fig. 5 and Table A5, Appendix A – Supplementary data). Recent work found that CA activity also occurs in soils and suggest that CA activity from *Actinobacteria and Proteobacteria* has a relevant role in soil carbon cycle (Meredith et al., 2018). Our results were consistent with those previously reported for grey microbial mats in Altamira Cave. In fact, Cuezva et al. (2012) described how the actinobacterial activity could be linked to the capture of CO_2 and proposed the reversible hydration of CO_2 by CA as a possible causal mechanism of CO_2 trapping and subsequent $CaCO_3$ precipitation. These CO_2 fixation mechanisms would be favored in stagnation stages with high concentrations of the gas, which diffuses freely through cell membranes and can be acquired by the moonmilk microbial community without a CO_2 concentrating mechanism. Also other known calcification mechanisms promoted by bacterial activity,

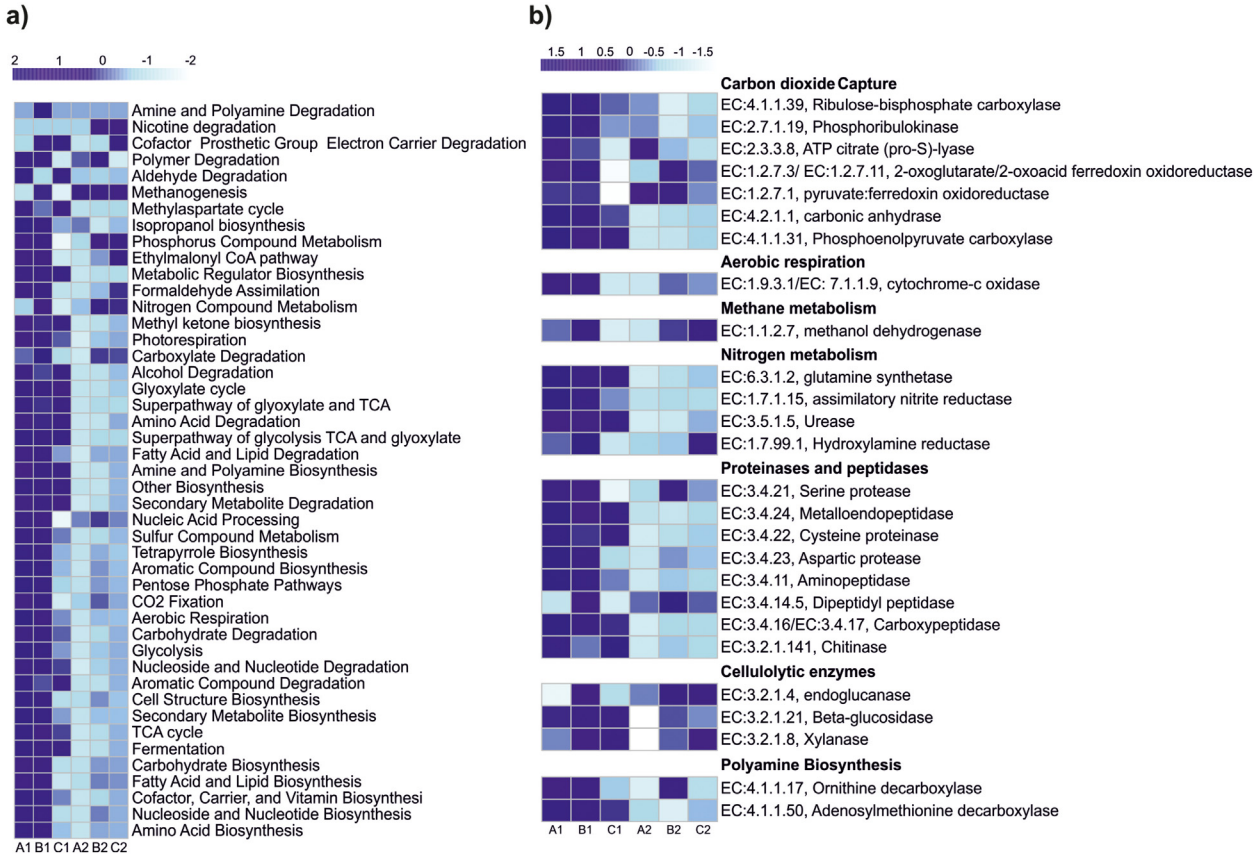

Fig. 5. Metagenome functions of moonmilk microbiota on CO_2, CH_4 and N cycles. (a) Heat-map showing the distribution of most abundant predicted ecological functions in PICRUSt2 (Y axis) in each sampling point (X axis). The dendrogram on top shows the clustering of samples. (b) Heat-map showing the normalized relative abundances of PICRUSt2 predicted genes (Y axis) encoding a selection of enzymes involved in carbon, methane and nitrogen cycles based on Metacyc database for each sampling point (X axis). Colors from white to dark blue designate the least abundant to most abundant.

such as ureolysis, ammonification and CO_2 capture by polyamines (Yasumoto et al., 2014; Maciejewska et al., 2017), were predicted by PICRUST, but only peptide/amino acid ammonification was associated to *Actinobacteria* (Fig. 5 and Tables A5–A6, Appendix A – Supplementary data). Ammonification produces CO_2 and NH_3 and may be related to carbonate precipitation of moonmilk as has been previously proposed (Maciejewska et al., 2017). In addition, our results revealed a higher relative abundance of wb1-P19 chemoautotrophic nitrite-oxidizing bacteria in the moonmilk deposits (Holmes et al., 2001). The *Proteobacteria* ASV wb1-P19 was predicted to contain ribulose-bisphosphate carboxylase and phosphoribulokinase, central enzymes in carbon fixation Calvin cycle, which could reduce the net flux of CO_2 by to autotrophic CO_2 fixation (Fig. 5 and Table A5, Appendix A – Supplementary data). Other chemoautotrophic nitrifying bacteria, with lower abundances in all samples, included the genus *Nitrospira* and the family *Nitrosomonadaceae*. Nitrifying bacteria have been reported as primary producers in caves, fixing CO_2 as the main carbon source and transforming ammonia to nitrate (Chen et al., 2009). Together, the results suggest that wb1-P19 and *Crossiella* could be one of the main responsible of observed negative CO_2 fluxes in moonmilk samples.

To get an accurate assessment and quantification of microbial processes in the C-GHG measurement in each period, a geochemical tracing of the gases was performed to distinguish between the different sources. A Keeling approach was conducted for tracking the CO_2 dynamics in the subterranean environment under two opposite gas-exchange settings with the exterior: ventilation and stagnation stages. This analysis revealed a CO_2 source from the bare cave sediments (δ^{13}C-CO2 = − 21.65‰; Fig. 6a) that was quite distinct from the lighter CO_2 degassed from moonmilk deposits ($\delta^{13}C$ = −25.58‰).

The lighter CO_2 sourced from moonmilk deposits most likely resulted from microbial induced calcite precipitation (MICP) and subsequent CO_2 degassing. The moonmilk bacterial metabolism promotes the calcite saturation of interstitial water, retained in the network of microbial mats and calcite fibers, which leads to preferential precipitation of the heavier carbon species (i.e., $Ca^{13}CO_3$) and subsequent increase of the lighter $^{12}CO_2$ in the interstitial water. This dissolved CO_2 is degassed into the cave atmosphere, which is favored during the ventilation stage when the colder and drier air from outside enters the cave environment. The $\delta^{13}C_{bulk}$ of the well-developed moonmilk (samples A1; Fig. 5) yields a value of −19.80 (± 0.17) ‰ (Table A7, Appendix A – Supplementary data). This considerably heavier value compared to carbon isotope composition of the emerging moonmilk and bare sediment surfaces is in concordance with MICP.

In contrast to CO_2, CH_4 was taken up (net negative flux) from the cave atmosphere by each of the deposits in both the ventilation and stagnation stage (Table 1). At the Pindal Cave, atmospheric CH_4 that enters the cave via advection through the cave entrance and other wide fissures and fractures, is the main CH_4 input. The residual CH_4 after the uptake-fluxes of atmospheric CH_4, becomes progressively depleted in ^{12}C, with $\delta^{13}C$-CH_4 values increasing from about −50‰ (freshly entered CH_4) towards −45 to −40‰ during the ventilation stage and even above −35‰ during the stagnation stage when atmospheric CH_4 influx is retarded (Fig. 6b). The continuous grey curves in Fig. 6b show the locus of compositions formed by methanotrophic consumption of atmospheric CH_4 modelled as a Rayleigh process with kinetic fractionation factors ranging from 1.0020 to 1.0273. The calculated kinetic fractionation factors associated with CH_4 oxidation in the cave deposits vary from 1.008 to 1.027, which are within the range reported for the aerobic oxidation of CH_4 in laboratory cultures of methanotrophs (Whiticar, 1999; Grant and Whiticar, 2002) and in in-situ

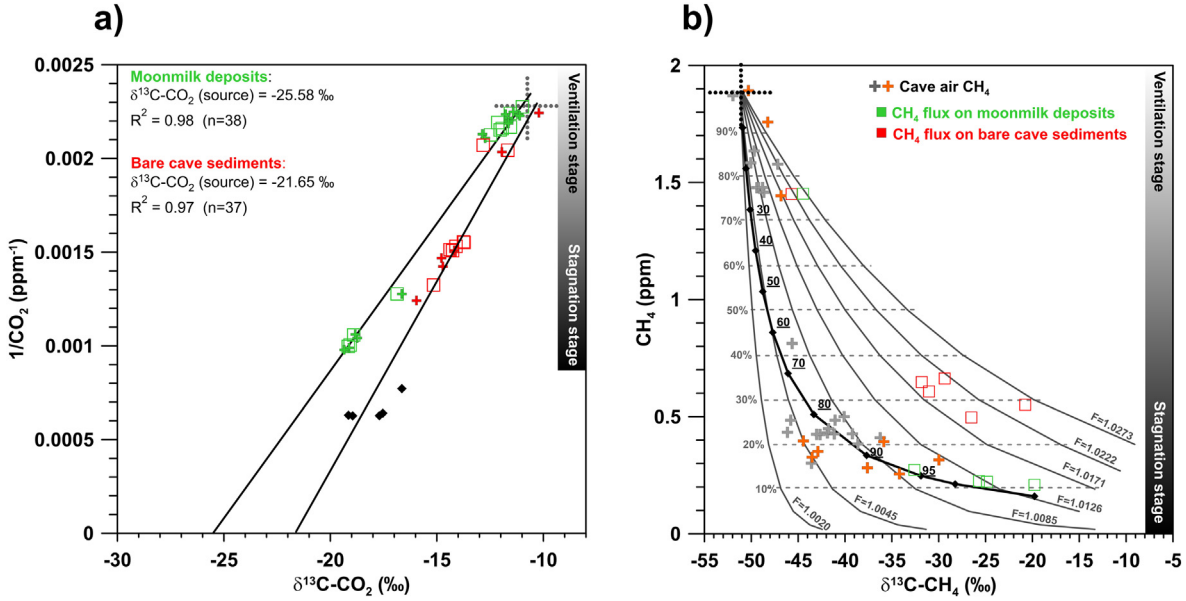

Fig. 6. (a) Keeling diagrams [δ^{13}C-CO_2 (‰) vs 1/CO_2 (ppm^{-1})]; (b) Relationship between CH_4 and δ^{13}C-CH_4 in cave air. CO_2 and CH_4 sourcing and exchange processes are studied in two microenvironments: bare cave sediments (red symbols) and moonmilk deposits (green symbols). Data set includes cave air (colored crosses), gases accumulated in the chamber coupled to the Gas Flux measuring system after registering the efflux or uptake by each microenvironment (open squares) and CO_2 stored in the sediments pore system sampled in both stages (closed black diamonds). Cave air samples were grouped in two pools for CH_4; those collected in the zone where gas flux measurements on the cave sediments were conducted (orange crosses) and those collected in the rest of cave locations (grey crosses). The dotted crosshairs represent the average CO_2 and CH_4 of the local atmosphere. See text for discussion about the fitted linear functions and curves modelling the CO_2 and CH_4 dynamic.

measurements on soils (Reeburgh et al., 1997; Maxfield et al., 2008) and in other vadose zone settings (Urmann et al., 2008; Mattey et al., 2013; Fernandez-Cortes et al., 2018). These results are fully consistent with subsurface environments acting as cleaning filters for atmospheric CH_4, on time scales ranging from hours to days, according to observations reported in previous studies (Fernandez-Cortes et al., 2015a; McDonough et al., 2016; Waring et al., 2017). The horizontal dotted lines with labels in Fig. 6b show the percentage of atmospheric CH_4 remaining in cave air after methanotrophic consumption. The data set for Pindal Cave (Fig. 6b) reveals a 65–75% removal of the atmospheric CH_4 entering the subterranean atmosphere due to bacterial oxidation over bare cave sediments during the stagnation stage, fully in line with these previous studies. The removal percentage rises to 90% in the moonmilk deposits, indicating increased CH_4 uptake activity by these communities relative to those in the bare sediments. The ventilation stage entails an extensive cave air renewal, increasing the contribution of atmospheric CH_4 and, consequently, the percentage of CH_4 removal drops to nearly 25% after the gas uptake and oxidation by methanotrophs from both bare cave sediments and moonmilk deposits. Finally, the CH_4 of cave air is the result of the addition of atmospheric CH_4 and its mixing with the highly ^{12}C depleted residue of methanotrophic oxidation in the cave formations. Black-solid curve in Fig. 6b bounds the joint trend of both the CH_4 of cave air and the highly-fractionated residual CH_4 after intense methanotrophic activity on moonmilk deposits. This curve was fitted by considering a mixing process between the mean atmospheric CH_4 (1.91 ± 0.03 ppm, −51.21 ± 1.61‰) with the most fractionated CH_4 (nearly to 0.20 ppm and −20‰) accumulated into the closed-chamber for gas flux monitoring. The underlined labels of this mixing curve show the percentage of highly-fractionated residual CH_4 present in cave air after microbial oxidation on moonmilk deposits. During the stagnation stage, the cave air data is indeed consistent with such mixing and with proportions of between 80% and 95% of highly-fractionated residual CH_4 present in cave air after microbial oxidation on moonmilk deposits.

Methylomonaceae (phylum *Proteobacteria*) is the most abundant methanotrophic family but we also found sequences with abundances below 1% related to the methanotrophic groups *Methylomirabilaceae* and *Methylacidiphilaceae*, within the phyla *Candidatus* Rokubacteria and *Verrucomicrobia*, respectively (Fig. 5 and Table A8, Appendix A – Supplementary data). These methanotrophic communities may be the main responsible for this remarkable CH_4 consumption in Pindal Cave.

4. Conclusions

In summary, the composition of the underground air is strongly conditioned by the activity of the bacterial communities present in the cave sediments. Long-term flux measurements show a continuous one-way CO_2 efflux from cave sediments into the open cave atmosphere as well as a continuous one-way CH_4 consumption from the cave air. Results also revealed significant seasonal variations in the magnitudes of the CO_2 and CH_4 fluxes, depending on the rate of air exchange between the underground environment and the external atmosphere (Table 1).

In sediments covered by moonmilk deposits, higher rates of CH_4 consumption and (during the stagnation stage) negative CO_2 fluxes were detected (Table 1 and Fig. 7). CO_2 capture was associated to *Crossiella* and the lineage wb1-P19, two predominant genera in the surface of sediments and specifically in moonmilk deposits, denoting an aerobic behavior. Carbonic anhydrases were the most abundant enzymes involved in CO_2 uptake, as predicted by metagenome inference, and their highest abundances were also connected to *Crossiella* and wb1-P19 lineage. The development of the aerial hyphae of *Actinobacteria* and the microbial extracellular polymeric substances formation facilitate the water retention in moonmilk. The precipitation of calcite and subsequently the moonmilk formation is favored by chemoautotrophic CO_2 fixation via the Calvin-Benson-Bassham cycle and by the capture of CO_2 by carbonic anhydrase in interstitial water. During ventilation stages, this phenomenon can be amplified by evaporation. Therefore, moonmilk (a ubiquitous and abundant deposit in underground environments) appears to be an evolved phase of the microbial processes in sediments where excess CO_2 is fixed as calcite and CH_4 oxidation was further intensified. In other words, moonmilk is a remarkable effective deposit in carbon sequestration.

Cave sediments act as surface soils with respect to their dynamics in a subterranean ecosystem involving not only the carbon cycle but also the

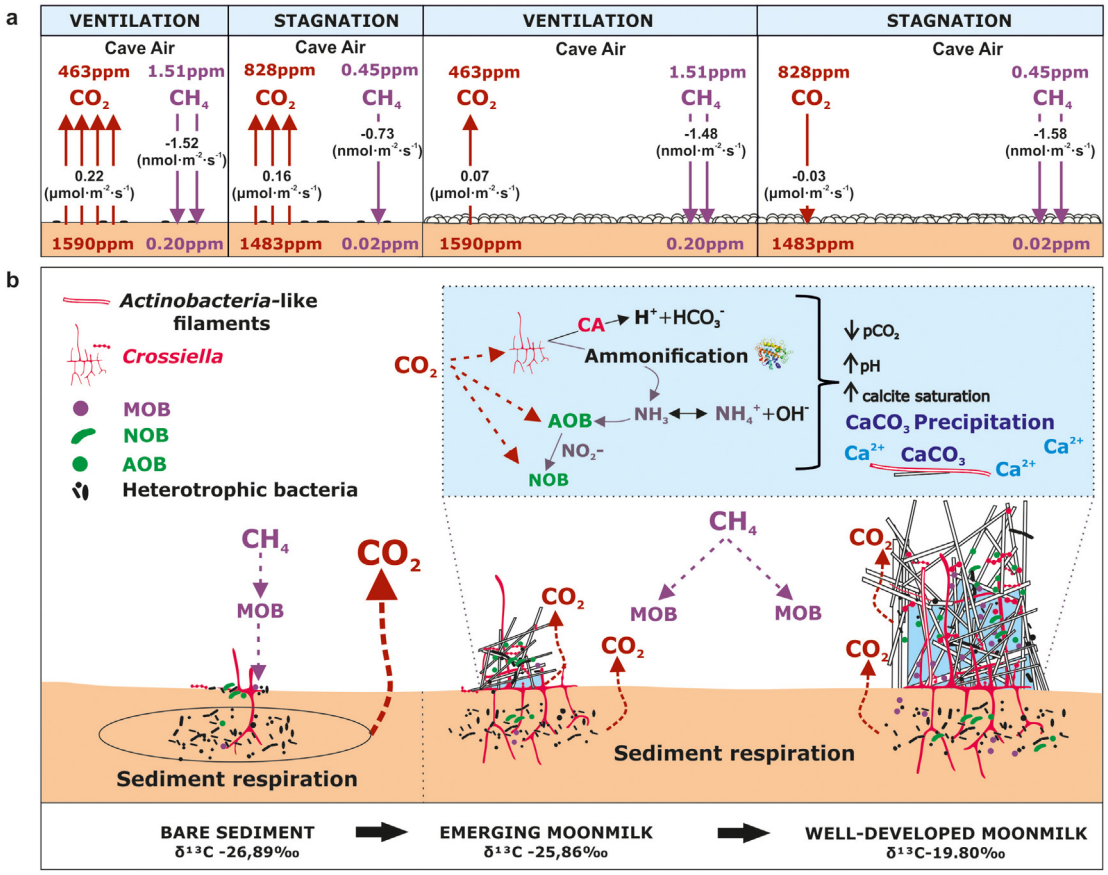

Fig. 7. Illustration of biogeochemical processes and greenhouse gas dynamic in Pindal Cave. (a), Carbon fluxes over cave sediments covered by moonmilk deposits and bare cave sediments during the cave ventilated and stagnation stages. Gas concentration in the cave and sediment air (ppm); carbon fluxes on average (μmol·m^{-2}·s^{-1} for CO_2 and nmol·m^{-2}·s^{-1} for CH_4). (b), Scheme of moonmilk evolution model from bare sediment to well-developed moonmilk and the microbial processes involved in moonmilk formation and greenhouse gas dynamic (MOB: Methane oxidizing bacteria, NOB: Nitrite oxidizing bacteria, AOB: Ammonia-oxidizing bacteria, CA: Carbonic anhydrase). At the bottom of the figure the carbon isotopes composition ($\delta^{13}C_{bulk}$, expressed as V-PDB ‰) of moonmilk deposits and the most superficial layer of bare cave sediments.

nitrogen cycle (Fig. 7). The kinetic fractionation factors associated with CH_4 oxidation in the cave are within the range calculated for the aerobic oxidation of CH_4 from methanotrophs in laboratory cultures and those calculated from in-situ measurements on soils. Regarding CO_2, syntrophic relationships are established between bacteria that performed ammonification (production of NH_3 and CO_2) → nitrification → CO_2 capture and NH_3 consumption. The ammonification process (associated to heterotrophic activity of *Actinobacteria*) may be the main responsible for the production of NH_3 and pH regulation. This constant flux is used by ammonia oxidizing bacteria (*Nitrosomonadaceae*) that transform the NH_3 in the sediments and together with nitrite oxidizing chemoautotrophic bacteria *(Nitrospira* and wb1-P19*)* and *Crossiella* participate in CO_2 regulation.

Results reveal that cave sediments host a diversity of microorganisms involved in the major biogeochemical cycles. They provide crucial ecosystem services, including nutrient cycling and carbon sequestration, all of which affect directly to greenhouse gas emissions and climate regulation.

Author contributions

Conceptualization, S.S.-M., A.F-C., S.C. and T.M.-P.; investigation, T.M.-P., J.C.C., S.S.-M., A.F-C., S.C., V.J. and N.S.; writing—original draft preparation, T.M.-P., S.S.-M., A.F-C., S.C., J.C.C.; writing—review and editing, C.S.-J., D.B., I.J., J.C.C., T.M.-P., S.S.-M., A.F-C., S.C. All authors contributed to the interpretation of the data and provided significant input to the final manuscript. All authors have read and agreed to the published version of the manuscript.

Declaration of competing interest

The authors declare that they have no known competing financial interests or personal relationships that could have appeared to influence the work reported in this paper.

Acknowledgements

This work was supported by the Spanish Ministry of Science, Innovation through project PID2019-110603RB-I00, MCIN/AEI/FEDER UE/10.13039/501100011033 and with collaboration of projects RTI2018-099052-B-I00 and PID2020-114978GB-I00. This research has also received funding from the European Union's Horizon 2020 research and innovation programme under the Marie Skłodowska-Curie grant agreement No 844535 — MIFLUKE.

Appendix A. Supplementary data

Supplementary data to this article can be found online at https://doi.org/10.1016/j.scitotenv.2022.154921.

References

Amir, A., McDonald, D., Navas-Molina, J.A., Kopylova, E., Morton, J.T., Xu, Z.Z., et al., 2017. Deblur rapidly resolves single-nucleotide community sequence patterns. mSystems 2, e00191-16. https://doi.org/10.1128/mSystems.00191-16.

Bokulich, N.A., Kaehler, B.D., Rideout, J.R., Dillon, M., Bolyen, E., Knight, R., et al., 2018. Optimizing taxonomic classification of marker-gene amplicon sequences with QIIME 2's q2-

feature-classifier plugin. Microbiome 6, 90. https://doi.org/10.1186/s40168-018-0470-z.
Bolyen, E., Rideout, J.R., Dillon, M.R., Bokulich, N.A., Abnet, C., Al-Ghalith, G.A., et al., 2019. Reproducible, interactive, scalable and extensible microbiome data science using QIIME 2. Nat. Biotechnol. 37, 852–857. https://doi.org/10.1038/s41587-019-209-9.
Brantley, S.L., Goldhaber, M.B., Ragnarsdottir, K.V., 2007. Crossing disciplines and scales to understand the critical zone. Elements 3, 307–314. https://doi.org/10.2113/gselements.3.5.307.
Cañaveras, J.C., Cuezva, S., Sanchez-Moral, S., Lario, J., Laiz, L., Gonzalez, J.M., et al., 2006. On the origin of fiber calcite crystals in moonmilk deposits. Naturwissenschaften 93, 27–32. https://doi.org/10.1007/s00114-005-0052-3.
Cerling, T.E., Solomon, D.K., Quade, J., Bowman, J.R., 1991. On the isotopic composition of carbon in soil carbon dioxide. Geochim. Cosmochim. Acta 55, 3403–3405. https://doi.org/10.1016/0016-7037(91)90498-T.
Chen, Y., Wu, L., Boden, R., Hillebrand, A., Kumaresan, D., Moussard, H., et al., 2009. Life without light: microbial diversity and evidence of sulfur- and ammonium-based chemolithotrophy in Movile Cave. ISME J. 3, 1093–1104. https://doi.org/10.1038/ISMEJ.2009.57.
Chen, Z., Auler, A.S., Bakalowicz, M., Drew, D., Griger, F., Hartmann, J., et al., 2017. The World Karst Aquifer Mapping Project: concept, mapping procedure and map of Europe. Hydrogeol. J. 25, 771–785. https://doi.org/10.1007/s10040-016-1519-3.
Cuezva, S., Fernandez-Cortes, A., Porca, E., Pašić, L., Jurado, V., Hernandez-Marine, M., et al., 2012. The biogeochemical role of Actinobacteria in Altamira Cave, Spain. FEMS Microbiol. Ecol. 81, 281–290. https://doi.org/10.1111/j.1574-6941.2012.01391.x.
Davidson, E.A., 1995. Spatial covariation of soil organic carbon, clay content, and drainage class at a regional scale. Landsc. Ecol. 10, 349–362. https://doi.org/10.1007/BF00130212.
De Goeyse, S., Webb, A.E., Reichart, G.J., De Nooijer, L.J., 2021. Carbonic anhydrase is involved in calcification by the benthic foraminifer Amphistegina lessonii. Biogeosciences 18, 393–401. https://doi.org/10.5194/BG-18-393-2021.
Douglas, G.M., Maffei, V.J., Zaneveld, J., Yurgel, S.N., Brown, J.R., Taylor, C.M., et al., 2019. PICRUSt2: An Improved and Extensible Approach for Metagenome Inference. 672295. BioRxiv. https://doi.org/10.1101/672295.
Eichorst, S.A., Trojan, D., Roux, S., Herbold, C., Rattei, T., Woebken, D., 2018. Genomic insights into the Acidobacteria reveal strategies for their success in terrestrial environments. Environ. Microbiol. 20, 1041–1063. https://doi.org/10.1111/1462-2920.14043.
Fernandez-Cortes, A., Cuezva, S., Alvarez-Gallego, M., Garcia-Anton, E., Pla, C., Benavente, D., et al., 2015a. Subterranean atmospheres may act as daily methane sinks. Nat. Commun. 6, 7003. https://doi.org/10.1038/ncomms8003.
Fernandez-Cortes, A., Cuezva, S., Garcia-Anton, E., Alvarez-Gallego, M., Pla, C., Benavente, D., et al., 2015b. Changes in the storage and sink of carbon dioxide in subsurface atmospheres controlled by climate-driven processes: the case of the Ojo Guareña karst system. Environ. Earth Sci. 74, 7715–7730. https://doi.org/10.1007/s12665-015-4710-2.
Fernandez-Cortes, A., Perez-Lopez, R., Cuezva, S., Calaforra, J.M., Cañaveras, J.C., Sanchez-Moral, S., 2018. Geochemical fingerprinting of rising deep endogenous gases in an active hypogenic karst system. Geofluids 2018, 4934520. https://doi.org/10.1155/2018/4934520.
Ford, D., Williams, P., 2007. Karst Hydrogeology and Geomorphology. John Wiley & Sons, Chichester https://doi.org/10.1002/9781118684986.
Garcia-Anton, E., Cuezva, S., Fernandez-Cortes, A., Alvarez-Gallego, M., Pla, C., Benavente, D., et al., 2017. Abiotic and seasonal control of soil-produced CO2 efflux in karstic ecosystems located in Oceanic and Mediterranean climates. Atmos. Environ. 164, 31–49. https://doi.org/10.1016/j.atmosenv.2017.05.036.
Gonzalez-Pimentel, J.L., Martin-Pozas, T., Jurado, V., Miller, A.Z., Caldeira, A.T., Fernandez-Lorenzo, O., et al., 2021. Prokaryotic communities from a lava tube cave in La Palma Island (Spain) are involved in the biogeochemical cycle of major elements. PeerJ 9, e11386. https://doi.org/10.7717/peerj.11386.
Grant, N.J., Whiticar, M.J., 2002. Stable carbon isotopic evidence for methane oxidation in plumes above Hydrate Ridge,Cascadia Oregon Margin. Glob. Biogeochem. Cycles 16, 1124. https://doi.org/10.1029/2001GB001851.
Herlemann, D.P., Labrenz, M., Jürgens, K., Bertilsson, S., Waniek, J.J., Andersson, A.F., 2011. Transitions in bacterial communities along the 2000 km salinity gradient of the Baltic Sea. ISME J. 5, 1571–1579. https://doi.org/10.1038/ismej.2011.41.
Holmes, A.J., Tujula, N.A., Holley, M., Contos, A., James, J.M., Rogers, P., Gillings, M.R., 2001. Phylogenetic structure of unusual aquatic microbial formations in Nullarbor caves, Australia. Environ. Microbiol. 3, 256–264. https://doi.org/10.1046/j.1462-2920.2001.00187.x.
James, E.W., Banner, J.L., Hardt, B., 2015. A global model for cave ventilation and seasonal bias in speleothem paleoclimate records. Geochem. Geophys. Geosyst. 16, 1044–1051. https://doi.org/10.1002/2014GC005658.
Jiménez-Sánchez, M., Bischoff, J.L., Stoll, H., Aranburu, A., 2006. A geochronological approach for cave evolution in the Cantabrian Coast (Pindal Cave, NW Spain). Z. Geomorphol. 147, 129–141.
Kuzyakov, Y., 2006. Sources of CO2 efflux from soil and review of partitioning methods. Soil Biol. Biochem. 38, 425–448. https://doi.org/10.1016/J.SOILBIO.2005.08.020.
Le Quéré, C., Andrew, R.M., Friedlingstein, P., Sitch, S., Hauck, J., Pongratz, J., et al., 2018. Global carbon budget 2018. Earth Syst. Sci. Data 10, 2141–2194. https://doi.org/10.5194/essd-10-2141-2018.
Lennon, J.T., Nguyễn-Thùy, D., Phạm, T.M., Drobniak, A., Tạ, P.H., Phạm, N.Đ., et al., 2017. Microbial contributions to subterranean methane sinks. Geobiology 15, 254–258. https://doi.org/10.1111/gbi.12214.
Lex, A., Gehlenborg, N., Strobelt, H., Vuillemot, R., Pfister, H., 2014. UpSet: visualization of intersecting sets. IEEE Trans. Vis. Comput. Graph. 20, 1983–1992. https://doi.org/10.1109/TVCG.2014.2346248.
Li, Q., Zhang, B., Yang, X., Ge, Q., 2018. Deterioration-associated microbiome of stone monuments: structure, variation, and assembly. Appl. Environ. Microbiol. 84, e02680-17. https://doi.org/10.1128/AEM.02680-17.
Ma, L., Huang, X., Wang, H., Yun, Y., Cheng, X., Liu, D., et al., 2021. Microbial interactions drive distinct taxonomic and potential metabolic responses to habitats in karst cave ecosystem. Microbiol. Spectr. 9, e01152-21. https://doi.org/10.1128/Spectrum.01152-21.
Maciejewska, M., Adam, D., Naômé, A., Martinet, L., Tenconi, E., Calusinska, M., et al., 2017. Assessment of the potential role of streptomyces in cave moonmilk formation. Front. Microbiol. 8, 1181. https://doi.org/10.3389/fmicb.2017.01181.
Maciejewska, M., Całusińska, M., Cornet, L., Adam, D., Pessi, I.S., Malchair, S., et al., 2018. High-throughput sequencing analysis of the actinobacterial spatial diversity in moonmilk deposits. Antibiotics 7, 27. https://doi.org/10.3390/antibiotics7020027.
Magnabosco, C., Lin, L.H., Dong, H., Bomberg, M., Ghiorse, W., Stan-Lotter, H., et al., 2018. The biomass and biodiversity of the continental subsurface. Nat. Geosci. 11, 707–717. https://doi.org/10.1038/s41561-018-0221-6.
Mattey, D.P., Fisher, R., Atkinson, T.C., Latin, J.P., Durrell, R., Ainsworth, M., et al., 2013. Methane in underground air in Gibraltar karst. Earth Planet. Sci. Lett. 374, 71–80. https://doi.org/10.1016/j.epsl.2013.05.011.
Mattey, D.P., Atkinson, T.C., Barker, J.A., Fisher, R., Latin, J.-P., Durrell, R., Ainsworth, M., 2016. Carbon dioxide, ground air and carbon cycling in Gibraltar karst. Geochim. Cosmochim. Acta 184, 88–113. https://doi.org/10.1016/J.GCA.2016.01.041.
Mattey, D.P., Atkinson, T.C., Hoffmann, D.L., Boyd, M., Ainsworth, M., Durell, R., et al., 2021. External controls on CO2 in Gibraltar cave air and ground air: implications for interpretation of δ13C in speleothems. Sci. Total Environ. 777, 146096. https://doi.org/10.1016/j.scitotenv.2021.146096.
Maxfield, P.J., Evershed, R.P., Hornibrook, E.R.C., 2008. Physical and biological controls on the in situ kinetic isotope effect associated with oxidation of atmospheric CH4 in mineral soils. Environ. Sci. Technol. 42, 7824–7830. https://doi.org/10.1021/es800544q.
McDonough, L.K., Iverach, C.P., Beckmann, S., Manefield, M., Rau, G.C., Baker, A., et al., 2016. Spatial variability of cave-air carbon dioxide and methane concentrations and isotopic compositions in a semi-arid karst environment. Environ. Earth Sci. 75, 700. https://doi.org/10.1007/s12665-016-5497-5.
McMurdie, P.J., Holmes, S., 2013. Phyloseq: an R package for reproducible interactive analysis and graphics of microbiome census data. PLoS ONE 8, e61217. https://doi.org/10.1371/journal.pone.0061217.
Meredith, L.K., Ogée, J., Boye, K., Singer, E., Wingate, L., von Sperber, C., et al., 2018. Soil exchange rates of COS and CO18O differ with the diversity of microbial communities and their carbonic anhydrase enzymes. ISME J. 13, 290–300. https://doi.org/10.1038/s41396-018-0270-2.
Miller, A.Z., Garcia-Sanchez, A.M., Martin-Sanchez, P.M., Costa Pereira, M.F., Spangenberg, J.E., Jurado, V., et al., 2018. Origin of abundant moonmilk deposits in a subsurface granitic environment. Sedimentology 65, 1482–1503. https://doi.org/10.1111/sed.12431.
Nguyễn-Thuỳ, D., Schimmelmann, A., Nguyễn-Văn, H., Drobniak, A., Lennon, J.T., Tạ, P.H., et al., 2017. Subterranean microbial oxidation of atmospheric methane in cavernous tropical karst. Chem. Geol. 466, 229–238. https://doi.org/10.1016/j.chemgeo.2017.06.014.
Okyay, T.O., Rodrigues, D.F., 2015. Biotic and abiotic effects on CO2 sequestration during microbially-induced calcium carbonate precipitation. FEMS Microbiol. Ecol. 91, 17. https://doi.org/10.1093/femsec/fiv017.
Park, S., Cho, Y.-J., Jung, D., Jo, K., Lee, E.-J., Lee, J.-S., 2020. Microbial diversity in moonmilk of Baeg-nyong Cave,Korean CZO. Fronti. Microbiol. 11, 613. https://doi.org/10.3389/fmicb.2020.00613.
Pataki, D.E., Ehleringer, J.R., Flanagan, L.B., Yakir, D., Bowling, D.R., Still, C.J., et al., 2003. The application and interpretation of Keeling plots in terrestrial carbon cycle research. Glob. Biogeochem. Cycles 17, 1022. https://doi.org/10.1029/2001GB001850.
Quast, C., Pruesse, E., Yilmaz, P., Gerken, J., Schweer, T., Yarza, P., et al., 2013. The SILVA ribosomal RNA gene database project: improved data processing and web-based tools. Nucleic Acids Res. 41, D590–D596. https://doi.org/10.1093/nar/gks1219.
Reeburgh, W.S., Hirsch, A.I., Sansone, F.J., Popp, B.N., Rtjst, T.M., 1997. Carbon kinetic isotope effect accompanying microbial oxidation of methane in boreal forest soils. Geochim. Cosmochim. Acta 61, 4761–4767. https://doi.org/10.1016/S0016-7037(97)00277-9.
Riquelme, C., Hathaway, J.J.M., Dapkevicius, M.L.N.E., Miller, A.Z., Kooser, A., Northup, D.E., et al., 2015. Actinobacterial diversity in volcanic caves and associated geomicrobiological interactions. Front. Microbiol. 6, 1342. https://doi.org/10.3389/fmicb.2015.01342.
Sánchez-Fernández, D., Galassi, D.M.P., Wynne, J.J., Cardoso, P., Mammola, S., 2021. Don't forget subterranean ecosystems in climate change agendas. Nat. Clim. Chang. 11, 458–459. https://doi.org/10.1038/s41558-021-01057-y.
Steger, F., Reich, J., Fuchs, W., Rittmann, S.K.-M.R., Gübitz, G.M., Ribitsch, D., et al., 2022. Comparison of carbonic anhydrases for CO2 sequestration. Int. J. Mol. Sci. 23, 957. https://doi.org/10.3390/ijms23020957.
Supuran, C.T., Capasso, C., 2017. An overview of the bacterial carbonic anhydrases. Metabolites 7, 56. https://doi.org/10.3390/metabo7040056.
Urmann, K., Schroth, M.H., Noll, M., Gonzalez-Gil, G., Zeyer, J., 2008. Assessment of microbial methane oxidation above a petroleum-contaminated aquifer using a combination of in situ techniques. J. Geophys. Res. Biogeosci. 113, G02006. https://doi.org/10.1029/2006JG000363.
Walkley, A., Black, I.A., 1934. An examination of the degtjareff method for determining soil organic matter and a proposed modification of the chromic acid titration method. Soil Sci. 37, 29–38. https://doi.org/10.1097/00010694-193401000-00003.
Waring, C.L., Hankin, S.I., Griffith, D.W.T., Kertesz, M.A., Kobylski, V., Wilson, N.L., et al., 2017. Seasonal total methane depletion in limestone caves. Sci. Rep. 7, 8314. https://doi.org/10.1038/s41598-017-07769-6.
Whiticar, M.J., 1999. Carbon and hydrogen isotope systematics of bacterial formation and oxidation of methane. Chem. Geol. 161, 291–314. https://doi.org/10.1016/S0009-2541(99)00092-3.
Yang, G., Li, L., Li, F., Zhang, C., Lyu, J.J., 2021. Mechanism of carbonate mineralization induced by microbes: taking Curvibacter lanceolatus strain HJ-1 as an example. Micron 140, 102980. https://doi.org/10.1016/j.micron.2020.102980.
Yasumoto, K., Yasumoto-Hirose, M., Yasumoto, J., Murata, R., Sato, S., Baba, M., et al., 2014. Biogenic polyamines capture CO2 and accelerate extracellular bacterial CaCO3 formation. Mar. Biotechnol. 16, 465–474. https://doi.org/10.1007/S10126-014-9566-z.